

# Land Cover and Its Impact on Monsoon Precipitation over South East Asia

Sudipta Sarkar  
George Mason University

Mentor: Dr. Christa Peters Lidard  
Hydrological Sciences Branch (Code 974)

**Abstract.** Global Vegetation Cover is strongly related to the climatic conditions. The strong effect of the rainfall has been found in controlling the global vegetation cover and agricultural crop yield. Based on the rainfall forecast the productivity of the crops and also the drought conditions are being monitored on routine basis. Land cover can also affect the regional to local climate regimes by governing the partitioning of heat balance terms and influencing soil moisture characteristics. This role of land cover in dictating climate change has been more difficult to establish and is found to give conflicting results worldwide. We try to assess the possible effect of land cover and attendant moisture flux over the monsoon rainfall in South East Asia where land cover has undergone some rapid and significant change in the past few years. Our work combines observational and analytical methods with modeling techniques to focus on key land cover class and specific areas that are likely to influence rainfall pattern and magnitude.

## 1. Introduction

Land-cover change - manifested as a change in surface greenness or change in vegetation pattern – is linked in complex and interactive ways to global climate change, and the feedback between the two exists at multiple spatial and temporal scales. The change in land cover influences climate and more specifically hydrological cycle through the partitioning of the incoming solar radiation into turbulent sensible and latent heat fluxes. The energy budget at the surface can be shown as follows (Pielke, 1984; Pielke, 2001)

$$R_N = Q_G + H + L(E + T) \quad (1)$$

$$P = E + T + RO + I \quad (2)$$

where  $R_N$  represents the net radiative fluxes  $= Q_S(1 - A) + Q_{LW}^{\downarrow} - Q_{LW}^{\uparrow}$ ,  $P$  is the precipitation,  $E$  is the evaporation,  $T$  is transpiration,  $Q_G$  is the soil heat flux,  $H$  is the turbulent sensitive heat flux,  $L(E+T)$  is the total turbulent latent heat flux term,  $RO$  is runoff,  $I$  is infiltration,

$Q_S$  is insolation,  $A$  is surface albedo,  $Q_{LW}^{\downarrow}$  is the downwelling longwave radiation and  $Q_{LW}^{\uparrow}$  is the upwelling longwave radiation. Any change in land cover is likely to change  $H$  and  $L(E+T)$  and affect the turbulent buoyant flux and development of the boundary layer. Evidences of such impact of land cover on regional climate pattern have been found in a number of studies worldwide (Charney et al., 1977; Courel et al., 1984; Shukla et al., 1990; Xue and Shukla, 1993). The potential role of anthropogenic vegetation changes has been investigated using global climate models (GCMs) in several sensitivity experiments (Chase et al., 1996; Zeng et al. 1999; Zeng and Neelin, 2000).

Studies carried out in different parts of the world have found contrasting results for the sensitivity of climate and hydrological cycle to different land cover. In a sensitivity experiment to identify the importance of land surface conditions on thunderstorm development in the Oklahoma-Texas Panhandle region, Pielke et al. (1997) have

found substantial effect of land surface comprising irrigated crops, short grass and shrubs in influencing cumulus cloud development compared to a landscape of just short grass. Lyons et al. (1993, 1996) and Huang et al. (1995) on the contrary have found a decrease in rainfall because of reduce sensible heat flux when the natural vegetation (short grass of prairies) was replaced by agriculture in Oklahoma area. De Ridder and Gallée (1998) found significant increase in convective rainfall in southern Israel associated with irrigation and intensification of agricultural practices, while De Ridder (1998) found that dense vegetation produces a positive feedback to precipitation. In this paper, we have made an attempt to delineate the land cover class over SEA region which has maximum influence on monsoon rainfall. We also try to assess the spatial and temporal scales of such coupling over SEA and the sensitivity of land cover change on monsoon rainfall.

## 2. Motivation for the Present Study

The primary goal of this study is to assess the effect of land cover on summer precipitation over the South East Asia (SEA). Initial investigation using observational data and time series analysis techniques reveals a consistent pattern in the coupling of land cover and summer rainfall that forms the key motivation of a further modeling study. The different analysis procedures and the salient observations are outlined below with an aim to emphasize the need for modeling the physics of such interaction that forms the focus of this report.

The observational framework covers a period of 19 years from 1982-2000 and makes use of two key data sources:

1. The modified NDVI data (version 3) from the Climate and Vegetation Research Group of Boston University ([ftp://crsa.bu.edu/pub/rmyneni/myneni/products/AVHRR\\_DATASETS/PAT\\_HFINDER](ftp://crsa.bu.edu/pub/rmyneni/myneni/products/AVHRR_DATASETS/PAT_HFINDER)). This data is an

improvement on the original Pathfinder AVHRR data and is corrected for any residual noise due to orbital drift, inter-sensor variations and stratospheric aerosol effects.

2. Monthly global rainfall mean produced by the Global Precipitation Climatology Project (GPCP) (<http://precip.gsfc.nasa.gov>) (Adler et al., 2003).
3. The coupling between land cover and rainfall over SEA have been explored for each pertinent land cover class as derived from the global land cover map by DeFries and Townshend (1994). The monthly average values of SOI are obtained for the period January, 1982 to December, 2000. The Dipole Mode Index (DMI) (Saji et al., 1999) is estimated from the data available from NCEP/NCAR reanalysis project (<http://iridl.ldeo.columbia.edu/SOURCES/NOAA/NCEP-NCAR/>) for January 1982 to December 2000. The soil moisture (SM) and land surface temperature (LST) are obtained from NCEP/NCAR reanalysis while the aerosol optical depth (AOD) comes from TOMS observations.

Figure 1 shows the first two modes of a combined EOF analysis (CEOF) estimated by maximizing the covariance between the normalized and deseasonalized estimates of NDVI and rainfall. A strong coupling is seen between the vegetation and rainfall variability Western Ghats (WG-I), parts of the Indo-Gangetic plains (IG) and Eastern and North-Eastern India (ENE-I) near the Bay of Bengal, Eastern and North-Eastern China (ENE-C), Thailand (TH) and the Indonesian archipelago (IND-AR).

The result of a Fourier series decomposition following Eq 1 and 2, of rain and vegetation at four different harmonics of 3, 6, 12 and 36 months respectively, are shown in figure 2.

$$G(x, y) = G(x, y)_{mean} + \sum_{r=1}^{r=N/2} [a_r \cos(2\pi r x / T) + b_r \sin(2\pi r x / T)] \dots\dots\dots (1)$$

where T = fundamental period of the data; T = 228 for 19 years of monthly data. N = the number of observations in the time series, R = the harmonic between 1 and N/2 and  $G(x, y)_{mean}$  = is the mean of the time series at the grid point (x,y) and  $a_r$  and  $b_r$  are the Fourier coefficients defined as:

$$a_r = 2 / N \sum_{x=1}^N [G(x, y) \sin(2\pi r x / T)]$$

$$b_r = 2 / N \sum_{x=1}^N [G(x, y) \cos(2\pi r x / T)]$$

(2)

are obtained from the Fourier decomposition mentioned above.

The coherency between rain and vegetation at grid locations where vegetation phase is found to lead rainfall are found to be significant at the annual and the inter-annual time scales. The same observation is confirmed through a cross correlation between the fundamental modes of rainfall and vegetation as obtained through an empirical mode decomposition. The coupling is seen to be stronger at time scales of 2-2.5 yrs and beyond.

The rainfall is corrected for any effect of El Nino, keeping in mind the significant correlation of the first mode of rainfall with SOI with 4 months lag ( $r = 0.89$ ,  $p = 0.0$ ). The seasonal composites of the anomalies of the two time series are then estimated at each grid point and the coefficient of variation (CV) is calculated for each time series and for each season. The cross correlation of these seasonal CV estimates of rainfall and vegetation for each land cover class (as derived by land cover classification of DeFries and Townshend 1994) shows that the MAM variability of “Cultivated Crops” is significantly correlated with the JJA rainfall (Table 1). A statistical sensitivity analysis and

a multiple linear regression analysis (MLR) of rainfall with vegetation and several other governing variables highlights two prominent areas in India and China as likely candidates for influencing rainfall (Figure 3). The average weighting fraction of each of the governing variables in the MLR formulation for JJA rainfall in areas of 70% or more explained variance is shown in table 2. The significant fraction of JJA rainfall that is seen to be explained by MAM SM suggests that the high amount of irrigation undertaken during MAM for the winter wheat crop grown in these areas may be the main factor.

### 3. A Modeling Approach

The high spatial and temporal coupling between rainfall and vegetation is seen to be dependent on specific land cover class and/or soil water content. The probable role of soil water content can be gauged by considering the growing cycle of winter wheat that is the staple crop to be sown during the beginning of winter season, in all areas of significant coupling discussed above. The wheat crop approaches its maturity around middle of March to first week of April thus necessitating the need for abundant irrigation in keeping with growing crop water requirement at this time and limited rainfall (Figure 4). This addition of moisture in the form of irrigation during MAM is likely to be retained by the soil and dictate the stability and convective cloud formation in the coming monsoon. Therefore we hypothesize that any role of land cover in influencing summer rainfall is due to:

1. The presence of a particular land cover (cropland, in our case)
2. The presence of anomalous amounts of soil moisture and water content.
3. A combination of both

The modeling approach aims to validate either or both of these hypotheses and justify the observations discussed in the previous section.

### 3.1 Methodology

The steps involved in modeling of the land surface feedback and subsequent impact on rainfall are shown in figure 5. Four primary experimental runs are defined to account for different changed scenarios and for a ten year period from 1990-1999 and at a  $0.25^{\circ}$  by  $0.25^{\circ}$  spatial grids. The study domain is restricted to our area of interest from  $20^{\circ}\text{S}$  to  $42^{\circ}\text{N}$  and from  $50^{\circ}\text{E}$  to  $141^{\circ}\text{E}$ .

- Run 1: The base run or the normal run wherein the present day scenario is simulated
- Run 2: Simulation with perturbed land cover. The relative role of cropland is examined by changing all crop classes to deciduous forests that were present over the areas of strong coupling before human interference (Ramankutty and Foley, 1999).
- Run 3: Examine the role of MAM soil water and irrigation by perturbing the input rainfall forcing to reflect the extra water that is brought in through irrigation. Four sub runs are defined under this particular run based on the method of choice for calculating the irrigation water requirement (IWR) and potential evaporation.

- ❖ IWR is calculated based on the difference between the potential evaporation and total evapotranspiration from vegetation as calculated by the land model. The evapotranspiration during growing season of crops is dominated by the transpiration from crops as the ground is shaded and thus only the total evapotranspiration from vegetation is concerned.

- ❖ The potential evaporation is calculated based on the formulation proposed by Penman-Monteith (PM). The actual evapotranspiration obtained from model run is subtracted from the potential term calculated through the PM approach to give the IWR.
- ❖ A FAO (Food and Agriculture Organization) approach to calculating the potential evaporation using the modified PM method using the reference evapotranspiration.
- ❖ A fourth simulation will be conducted under this scenario to take into account the effect of irrigation that is more what is necessarily required. This scenario is considered as in reality farmers have little knowledge of the exact crop water requirement and thus tend to over irrigate.
- Run 4: A simulation scenario where both the vegetation and rainfall have been perturbed to quantify the extent of impact of both on rainfall.

### 3.2 Choice of Model

We have chosen to work with the Community Land Model (CLM) as a part of our modeling study. This model has been developed as a collaborative venture between the different land modeling groups and combines the best features of three well documented and modular land models the Land Surface Model (LSM) of Bonan (1996), the Biosphere–Atmosphere Transfer Scheme (BATS) of Dickinson et al. (1993), and the 1994 version of the Chinese Academy of Sciences Institute of Atmospheric Physics LSM (IAP94) (Dai and Zeng 1997).

We chose CLM over other land modeling schemes like VIC and NOAH because CLM makes use of a better two leaf canopy model (Dai et al., 2004) (has separate

sun lit and shaded canopy fraction) compared to Noah and VIC that uses a single “big leaf” canopy model (Jarvis 1976). 2) CLM uses a more advanced coupled photosynthesis and water exchange model (Collatz et al., 1991) called the Ball and Berry model for calculating the stomatal conductance. This means CLM is better formulated for predicting CO<sub>2</sub> and water vapor exchanges than Noah and VIC that may overestimate these terms. CLM has better soil depth parameterization -soil temperature is predicted using a heat diffusion equation in 10 soil layers which is important as feedback and memory of the water table and “deep” ground processes is important to the surface water and energy budgets. It has a thinner and more realistic top soil layer (1.75 cms) compared which helps CLM better simulate surface soil water fluxes and the diurnal cycle of surface soil temperature. CLM is also likely to have improved annual cycle of runoff and hence evapotranspiration because of improved soil depth parameterizations.

### 3.3 *Data*

The data requirement for this modeling study serves three purposes:

1. Define the characteristic vegetation and topography for each grid of the land surface scheme. The respective datasets in this category are:
  - a. Global land cover from University of Maryland with 13 land classes (DeFries and Townshend 1994)
  - b. Global 16kms monthly climatological values of Leaf and Stem Area Indices from the department of Geography, Boston University.
  - c. Global soil color and texture dataset from NOAA (Reynolds et al., 1999)
2. Define the boundary atmospheric forcing conditions for offline run of the CLM land surface scheme. The

bias corrected NCEP/NCAR Reanalysis dataset (Berg et al., 2003) have been used in this study.

3. The need for constraining the model forcing data with actual observation. The assimilation of actual observations from satellite borne sensors, ground stations and gauges are important to constrain the magnitude of different geophysical variables within realistic limits. In our study the pentad rainfall estimates from the CPC Merged Analysis of Precipitation (CMAP) have been assimilated with the rainfall forcing from the NCEP/NCAR reanalysis. The pentad rainfall estimates are disaggregated to fit the reanalysis spatial and temporal resolution through a data disaggregation scheme outlined in the next section.

#### 3.3.1 *Pentad rainfall assimilation*

The main purpose of disaggregation and assimilation of observed rainfall data is to preserve the temporal pattern of rainfall over a grid through model estimates while at the same time constrain the cumulated hourly estimates with observed values. The disaggregation process consists of four steps;

- 5 days of 0.5 deg. 6hrly reanalysis forcing (R) -> 2.5 deg. 6hrly (A)
  - Average 2.5 deg. 6hrly (A) for 5 days -> 2.5 deg. CMAP pentad equivalent (B)
  - Disaggregate CMAP pentad data (P) to 2.5 deg 6 hrly (Q):
  - $Q = P \cdot (A/B)$
  - Interpolate Q to 0.5 deg. 6hrly Q'
- Q' is used instead of the actual forcing rainfall rate at each model time step.

## 4. **Model Results and Discussion**

Figure 6 (a-g) summarizes some of our findings from the first four model runs considering the normal scenario, perturbed vegetation (PV) , perturbed rainfall vis-à-vis

soil moisture (PR) and both (PV+PR) for a point located at 30N, 76E. It shows the behavior of the heat flux (latent and sensible heat), surface temperature, stability (obukhov length), moisture balance (soil water, potential and total evaporation from vegetation) for the four different boundary conditions. A thick deciduous forest cover is seen to give of more latent heat flux during summer (JJA) (figure 6a) compared to the present day land cover of crops and shrubs. The PV+PR case tops the release of latent heat flux and confirms more evaporative capability of forest canopy (figure 6 f, g) given their greater leaf area and more penetrative root zone. As a result of more evaporation through thicker stem and leaf foliage the forest cover tends to preserve less soil water (figure 6d). Conversely the thick forest cover tends to preserve the sensible heat (figure 6b) release from the ground given their thick canopy cover that protects the ground from direct solar heating. This leads to more heating of ground and more surface temperature than a more barren land with more loss of heat through convection and conduction.

The increase in latent heat flux by addition of more water during MAM is confirmed by the behavior of the PR and PR+PV rains. Both the curves show an increased release of latent heat flux and capacity for more sustained total evaporation from vegetation than their drier counterparts. The persistence of the soil moisture induced latent heat release during greater part of June is very significant and is likely to contribute to the development of moist instability within the monsoon air mass that arrives over the Indian land mass from the Indian Ocean. This persistence of soil moisture induced latent heat flux of nearly a month conforms to earlier findings regarding soil moisture memory over the subtropics (14N-33N) by Wu and Dickinson (2004). They had found a persistent time scale for soil moisture of 1.3-2 months in the top 0.5 m and 2.6-6.7 months for soil moisture in the deeper root zone, in

the subtropics. So it seems likely that the rise and persistence of latent heat release is largely the result of evapotranspiration from the top soil layers as wheat has very deep root structure during its growing stages. This increase in soil moisture is also likely to persist as the irrigation trend continues through the summer with the winter wheat crop making way for the sowing of summer rice.

Similar results have been obtained from other points located along the wheat belt of northern India discussed in previous sections. The behavior over Eastern China is a bit more complex and any strong increase in latent heat flux and evapotranspiration are lacking in response to increased soil moisture (not shown). This may indicate that more water is being lost as runoff, in keeping with the findings of Wu and Dickinson (figure 7, 2004). They had found lower cross correlation between evapotranspiration and soil moisture while higher values between runoff and soil moisture, over a crop land site located at 29N, 107E, similar to our study area location over China.

The monsoon rainfall over South Asia is the result of moist air masses that are carried over from the Indian and Pacific Ocean in response to the land sea thermal gradient that exists during summer. This overall precipitation pattern may be dictated at local to regional scales by the latent heat flux release and a moist and cooler atmospheric boundary layer. The results from the simulations over Indian sub-continent suggest that the change in land cover may have influenced the strengthening of monsoon by affecting both the processes mentioned above in two contradictory ways:

1. The strengthening of convective circulation because of higher sensible heat release brought about by a change over from the natural landscape consisting of forests to one consisting of crops and shrubs increases the chance of heavy showers and thunderstorms. The moisture laden

wind is more likely to be uplifted to the level of free convection under this scenario.

2. Strengthening of the rainfall associated with monsoon winds by aiding the development of regional instabilities by release of more latent heat and moisture into the lower

atmospheric boundary layer because of heavy use of irrigation.

The first process can only be of historical significance and in present days it's the second process that is possibly fine tuning the gross monsoon induced precipitation budget over South and South East Asia, dominantly over the Indian sub-continent.

## References:

- Adler, R.F., Huffman, G.J., Chang, A., Ferraro, R., Xie, P., Janowiak, J., Rudolf, B., Schneider, U., Curtis, S., Bolvin, D., Gruber, A., Susskind, J., Arkin, P. The Version 2 Global Precipitation Climatology Project (GPCP) Monthly Precipitation Analysis (1979-Present). *J. Hydrometeor.* 2, 36-50, 2003.
- Berg, A. A., Famiglietti, J.S., Walker, J.P., Houser, P.R. Impact of bias correction to reanalysis products on simulations of North American soil moisture and hydrological fluxes, *J. Geophys. Res.*, 108(D16), 4490, 2003
- Bonan, G. The NCAR land surface model (LSM version 1.0) coupled to the NCAR community climate model. Technical Report NCAR/TN-429 + STR, NCAR Boulder, Colorado, 1996.
- Charney, J. G., Quirk, W. J., Chow, S., Kornfield, J. A comparative study of the effects of albedo change on drought in the semiarid regions. *J. Atmos. Science* 34, 1366-1385, 1977.
- Chase T. N., Pielke R. A., Kittel, T.G.F., Nemani, R., Running, S. W. Sensitivity of a general circulation model to global changes in leaf area index. *J. Geophys. Res.* 101, 7393-7408, 1996.
- Collatz, G.J., Ball, J.T., Grivet, C., and Berry, J.A., Physiological and environmental regulation of stomatal conductance, photosynthesis, and transpiration: a model that includes a laminar boundary layer. *Agric. For. Meteorol.*, 54, 107-136, 1991.
- Courel, M., Kandel, R.S., Rasool, S.I. Surface albedo and the Sahel drought. *Nature* 307, 528-531, 1984.
- Dai, Y., Zeng, Q. A land surface model (IAP94) for climate studies, Part I: formulation and validation in off-line experiments. *Advances in Atmos. Sci.*, 14, 443-460, 1997.
- Dai, Y., Dickinson, R. E., Wang, Y.P., A Two-Big-Leaf Model for Canopy Temperature, Photosynthesis, and Stomatal Conductance. *Journal of Climate*: 17(12), 2281–2299, 2004.
- DeFries, R. S., Townshend, J. R. G. NDVI-derived land cover classification at a global scale. *Int. J. Remote Sensing* 15, 3567-3586, 1994.
- De Ridder, K. The impact of vegetation cover on Sahelian drought persistence. *Boundary Layer Meteorol.* 88, 307–321, 1998.
- De Ridder, K., Gallée, H. Land surface-induced regional climate change in southern Israel. *J. Appl. Meteorol.* 37, 1470–1485, 1998.

- Dickinson, R. E., Henderson-Sellers, A., Kennedy, P. J. Biosphere Atmosphere Transfer Scheme (BATS) Version 1e as Coupled to the NCAR Community Climate Model. NCAR Technical Note, NCAR, 72 pp, 1993.
- Huang, X., Lyons, T.J., Smith, R. C. G. Meteorological impact of replacing native perennial vegetation with annual agricultural species, in Scale Issues in Hydrological Modeling, edited by J. D. Kalma and M. Sivapalan, pp. 401-410, Advanstar Commun., Chichester, England, 1995.
- Jarvis, P.G. The interpretation of leaf water potential and stomatal conductance found in canopies in the field. *Phil. Trans. R. Soc. London*, Ser. B, 273, 593-610, 1976.
- Lyons, T. J., Schwerdtfeger, P., Hacker, J.M., Foster, I. J., Smith, R. C. G., Xinmei, H. Land-atmosphere interaction in a semiarid region: The bunny fence experiment. *Bull. Am. Meteorol. Soc.* 74, 1327-1334, 1993.
- Lyons, T. J., Smith, R. C. G., Xinmei, H. The impact of clearing for agriculture on the surface energy budget. *Int. J. Climatol.* 16, 551-558, 1996.
- Pielke, R. A. Mesoscale Meteorological Modeling, 612 pp., Academic, San Diego, California, 1984.
- Pielke, R. A. Influence of the spatial distribution of vegetation and soils on the prediction of cumulus convective rainfall. *Rev. Geophys.* 39, 151-177, 2001.
- Ramankutty, N., J.A. Foley. Estimating historical changes in land cover: North American croplands from 1850 to 1992. *Global Ecology and Biogeography* 8, 381-396, 1999.
- Reynolds, C. A., Jackson, T. J., Rawls, W. J. Estimating Available Water Content by Linking the FAO Soil Map of the World with Global Soil Profile Databases and Pedo-transfer Functions. Proceedings of the AGU 1999 Spring Conference, Boston, MA. May31-June 4, 1999.
- Saji, N.H., Goswami, B. N., Vinayachandran, P. N., Yamagata, T. A dipole mode in the tropical Indian Ocean. *Nature* 401, 360-363, 1999.
- Shukla, J., Nobre, C., Sellers, P. Amazon deforestation and climate change. *Science* 247, 1322-1325, 1990.
- Wu, W., Dickinson, R. E. Time Scales of Layered Soil Moisture Memory in the Context of Land Atmosphere Interaction. *Journal of Climate*, 17, 2752-2764, 2004.
- Xue, Y., Shukla, J. The influence of land surface properties on Sahel climate. Part I: Desertification. *J. Climate* 6, 2232-2245, 1993.
- Zeng, N., Neelin J. D., Lau, W. K. M., Tucker, C. J. Enhancement of interdecadal climate variability in the Sahel by vegetation interaction. *Science* 286, 1537-1540, 1999.
- Zeng, N., Neelin, J.D. The Role of Vegetation-Climate Interaction and Interannual Variability in Shaping the African Savanna. *J. Climate* 13, 2665-2670, 2000.

## Figure Captions

**Figure 1:** The first two principal modes of CEOF for NDVI (upper panel) and Rainfall (lower panel) are shown. EOF 1 explains about 29% of total variance while EOF 2 explains 10% of combined variance.

**Figure 2:** The spatial coherence plots between Rainfall and NDVI for the 3, 6, 12 and 36 months harmonics corresponding to S, SA, A, IA respectively. Only values significant at 95% have been shown for better representation.

**Figure 3:** The points showing areas of high explained variance ( $> 70\%$ ) of monsoon rainfall through a combination of land surface and climatological parameters. See text for further details. All values shown are significant at an alpha value of 0.05.

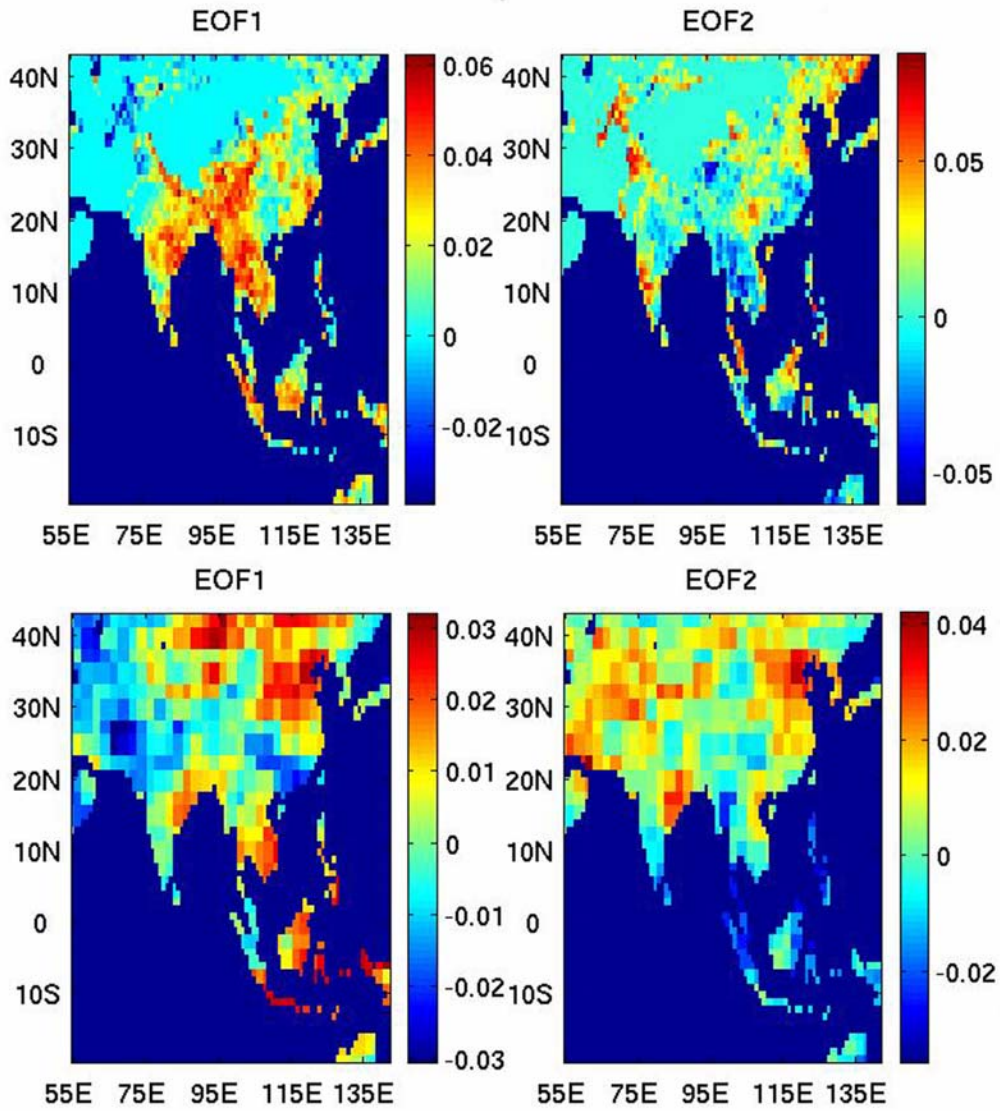
**Figure 4:** The need for irrigation is shown by the difference in magnitude between the crop water requirement, obtained as a (a) difference of potential and total evapotranspiration from vegetation (expressed in mm/day) and (b) MAM averaged rainfall (mm/day). (c) The areas where crop water demand is higher than MAM rainfall are seen to be the areas of maximum irrigation.

**Figure 5:** The flowchart showing the approach taken in the modeling validation of the observation result.

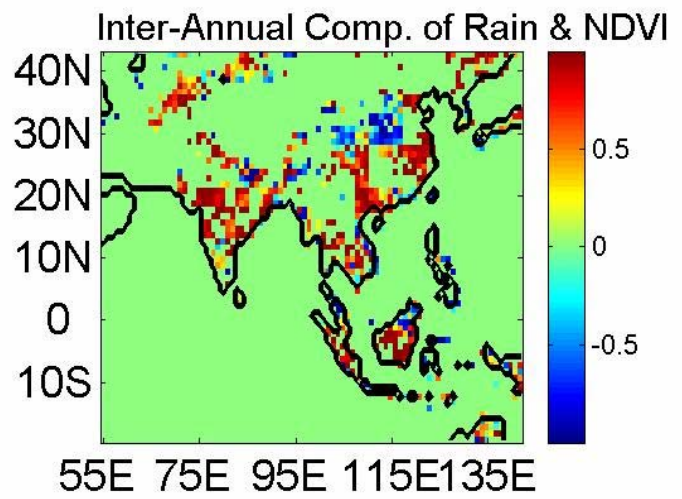
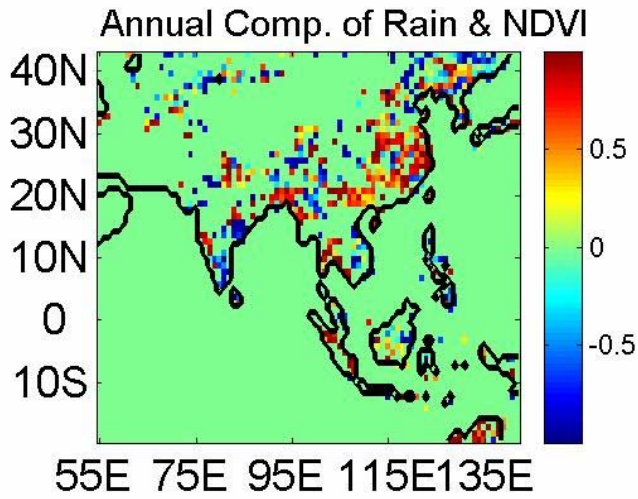
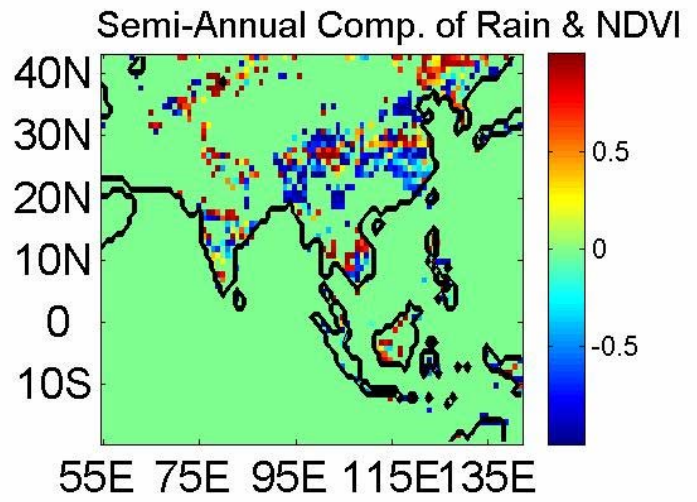
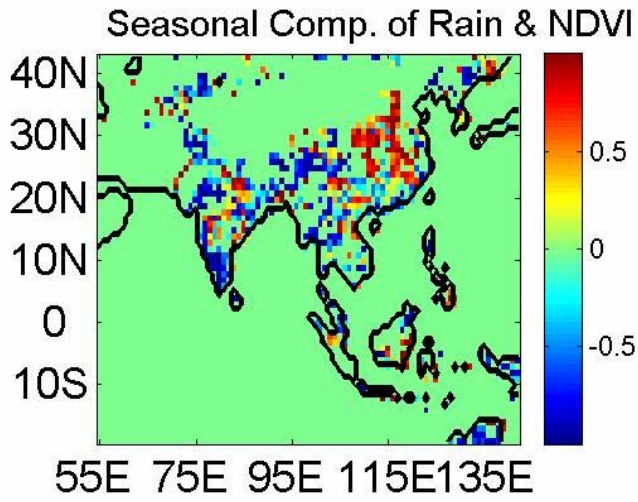
**Figure 6:** The daily mean of (a) latent heat, (b) sensible heat, (c) surface temperature, (d) soil wetness, (e) obukhov length, (f) total and (g) potential evaporation from vegetation, averaged over 7 years from 1992-1998. The runs are labeled as Normal, PV (Perturbed Vegetation), Perturbed Water (PW) and Perturbed Water + Vegetation (PW+PV)

# Figures

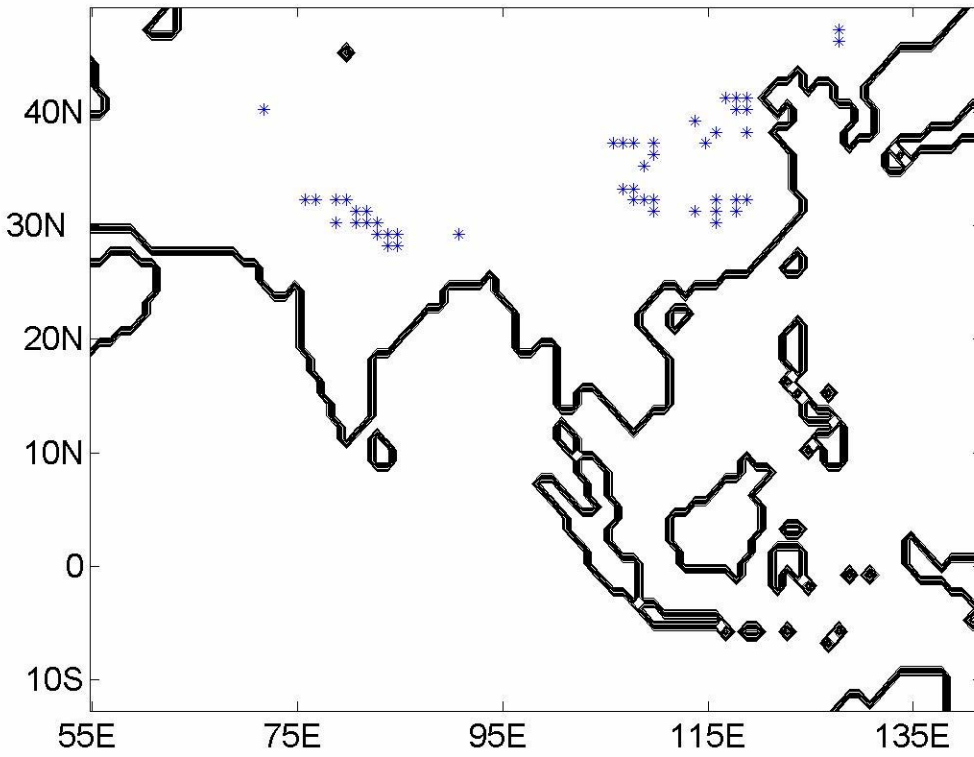
1.



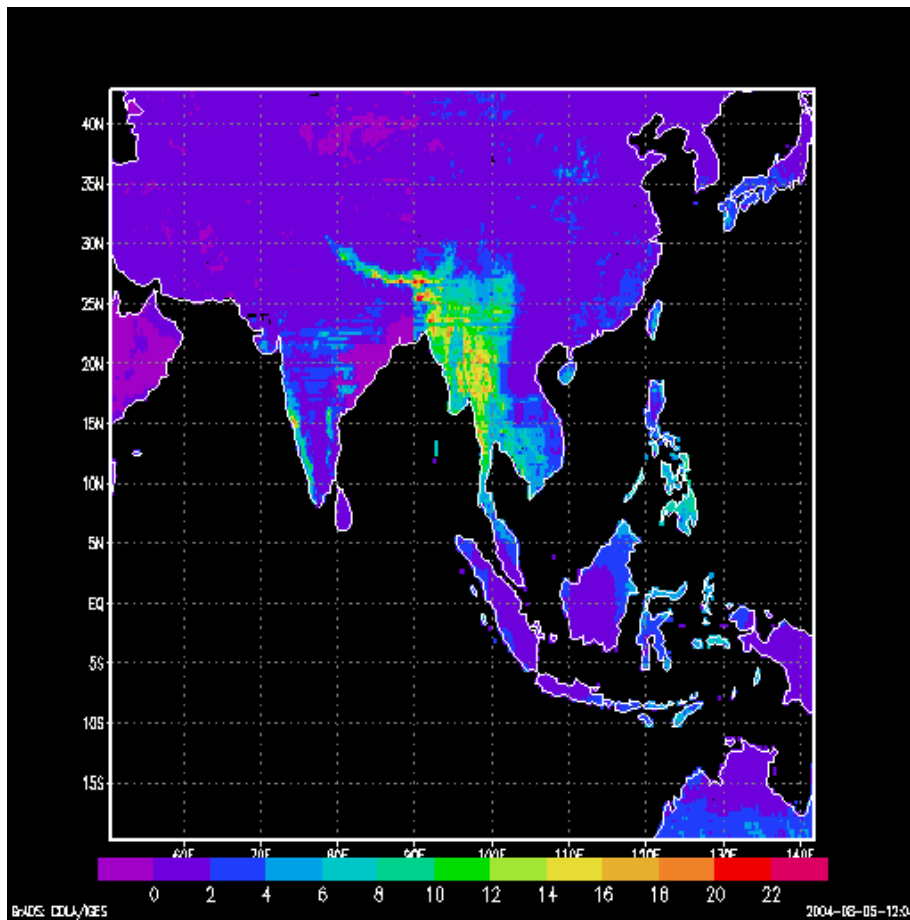
2.



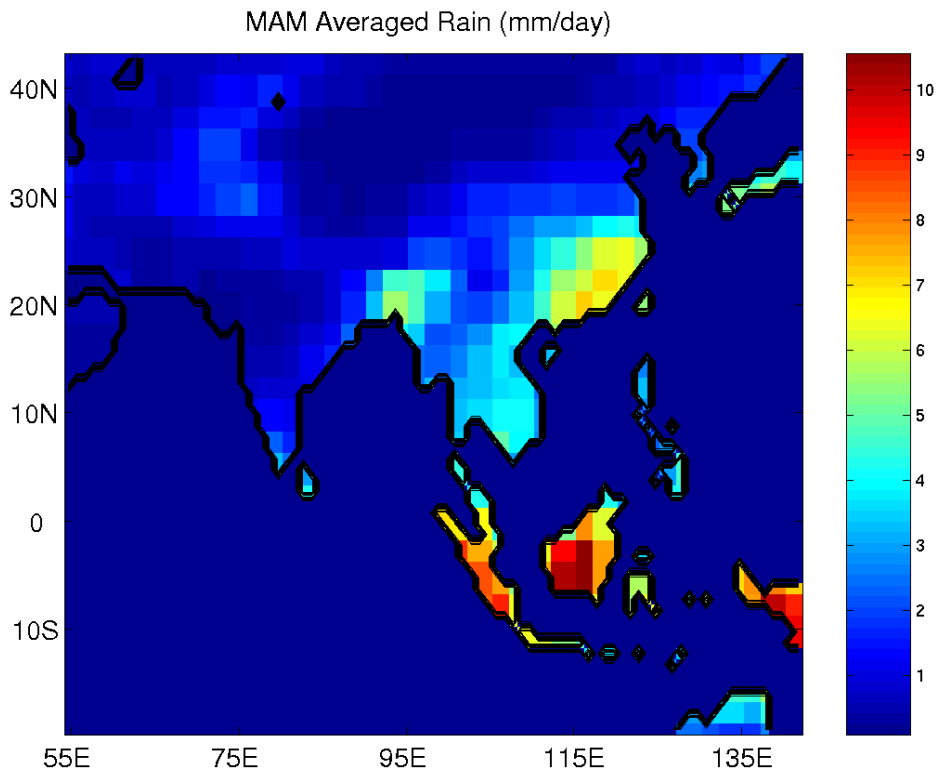
3.



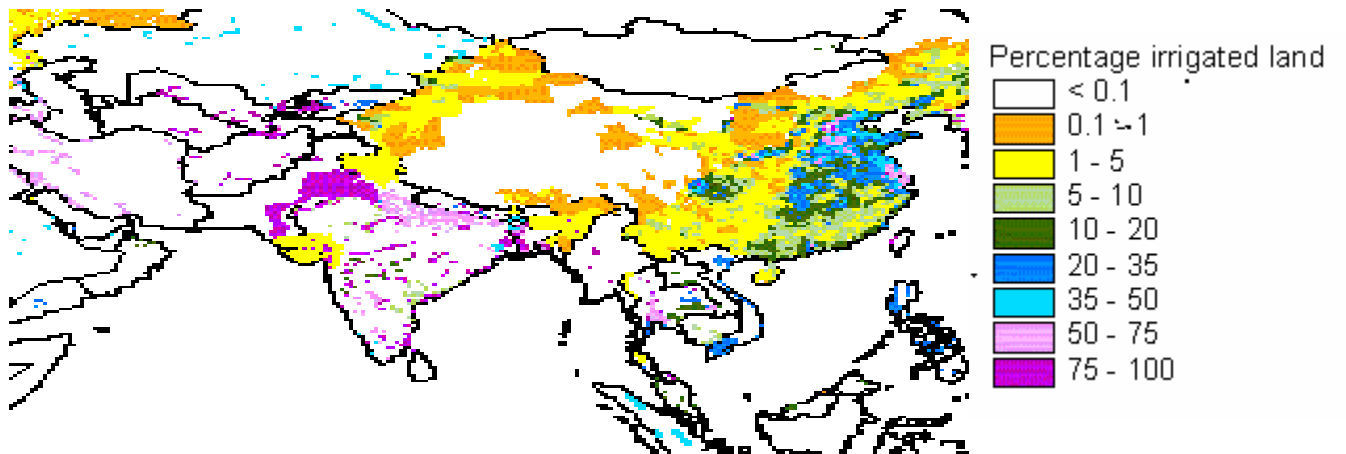
4a.



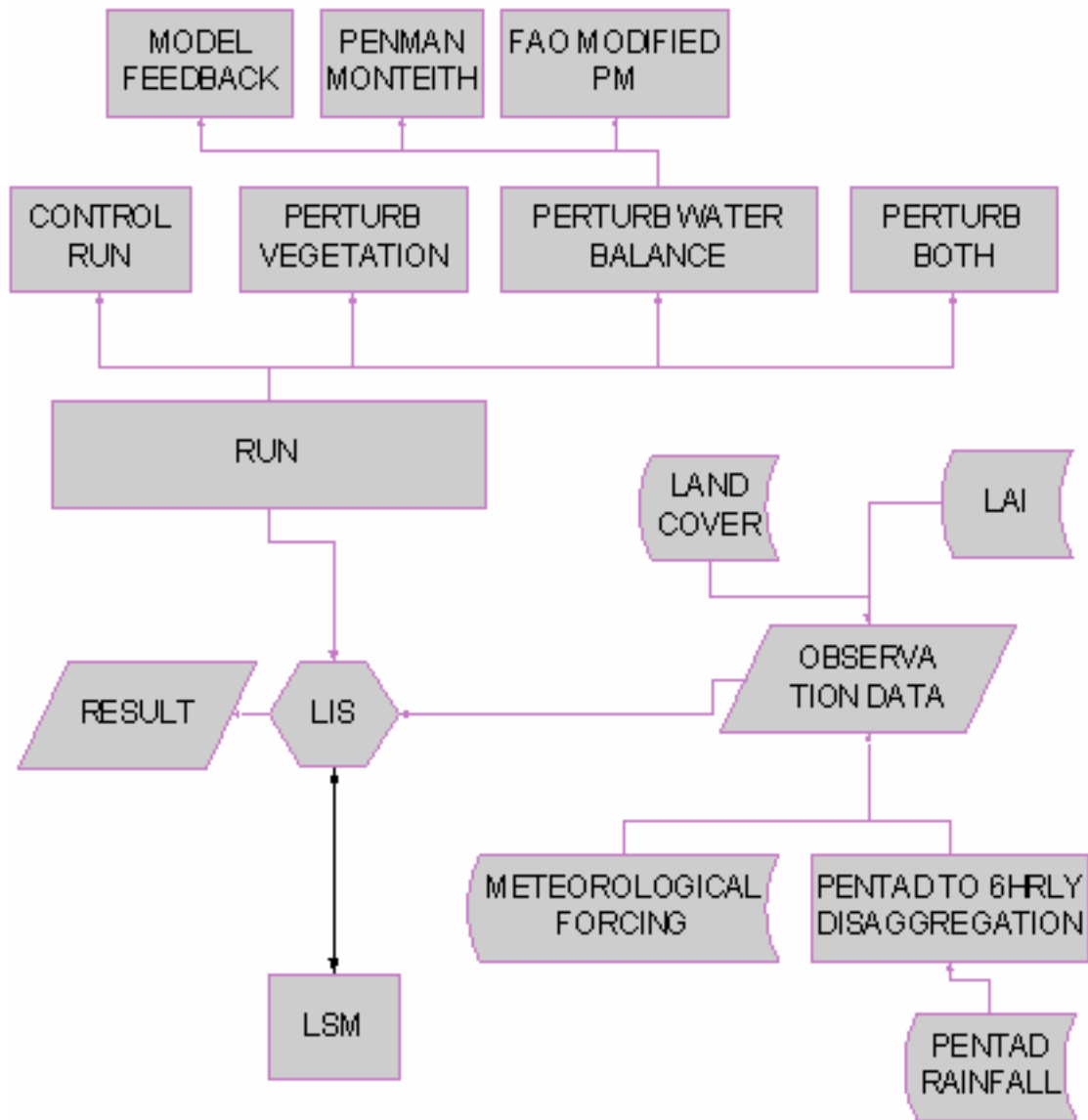
4b.



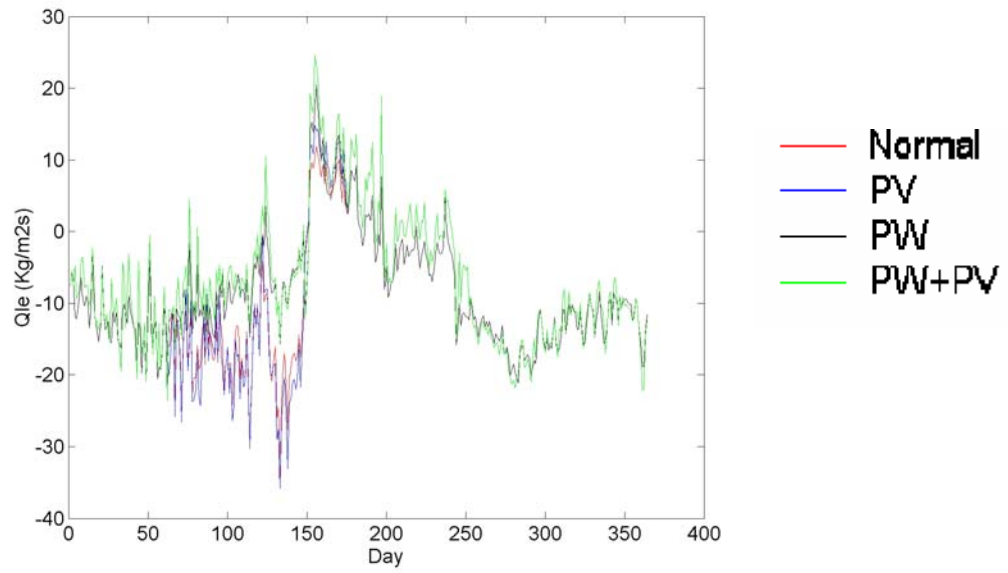
4c.



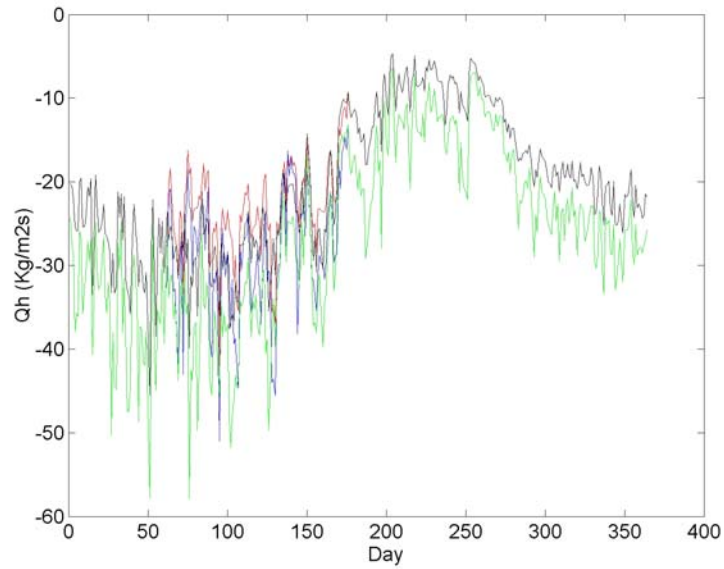
5.



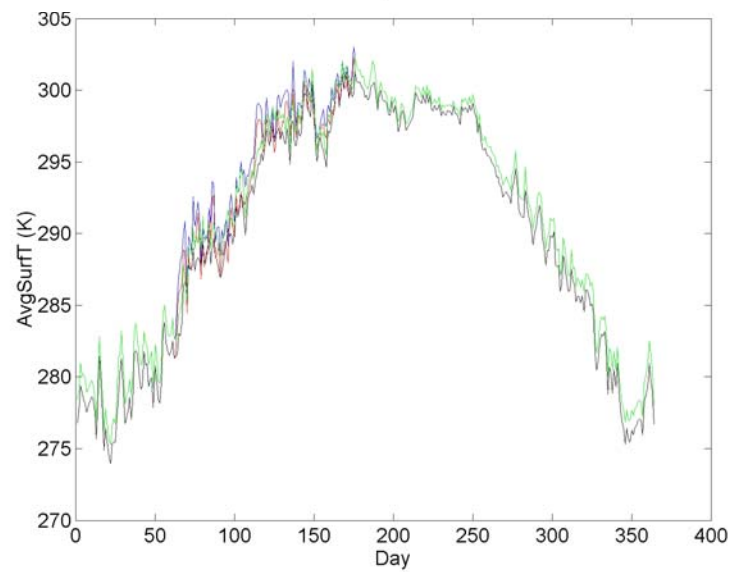
6a.



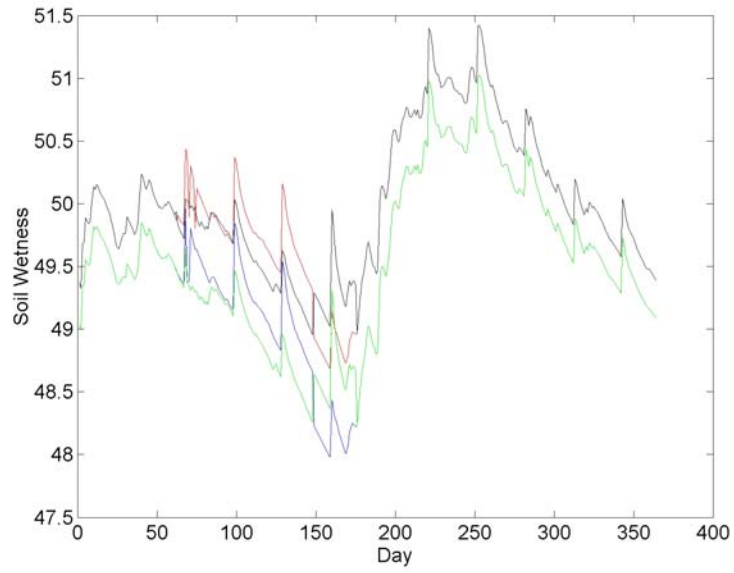
6b.



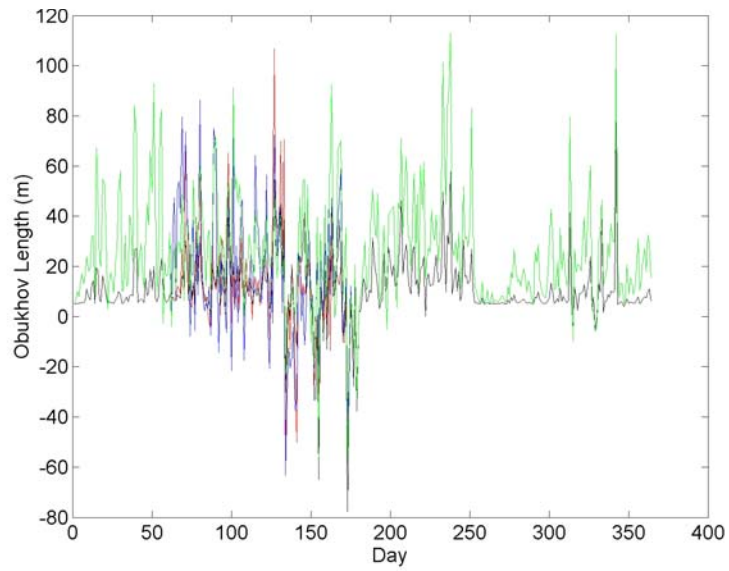
6c.



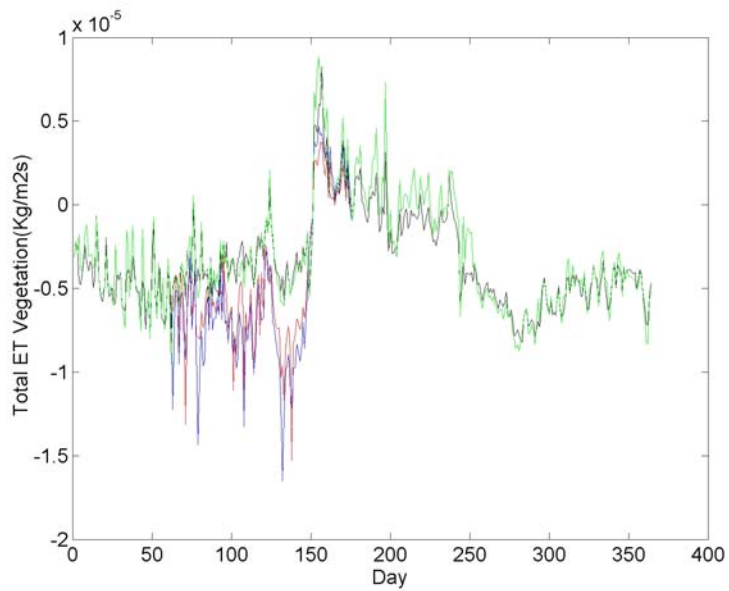
6d.



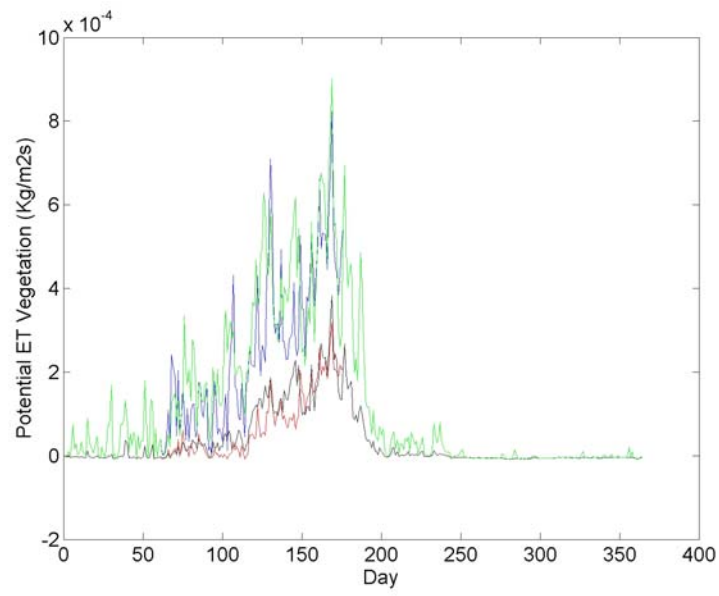
6e.



6f.



6g.



## Tables

**Table 1.** The correlation estimates between class composite CVs of rainfall and NDVI. Correlation estimates with associated p-values < 0.05 have been changed to zeros, and land-classes having no significant correlation values have been ignored.

<b>6. Wooded Grassland</b>	<b>DJF Rain</b>	<b>MAM Rain</b>	<b>JJA Rain</b>	<b>SON Rain</b>
DJF_NDVI	0	0	0	0
MAM_NDVI	0	0	0	0
JJA_NDVI	0	0	0	0
SON_NDVI	0	0	<b>0.58</b>	0
<b>7. Grassland</b>				
DJF_NDVI	0	0	0	0
MAM_NDVI	0	0	0	0
JJA_NDVI	0	0	0	0
SON_NDVI	0	0	<b>0.51</b>	0
<b>10. Cultivated Crops</b>				
DJF_NDVI	0	0	0	0
MAM_NDVI	<b>0.47</b>	0	<b>0.54</b>	0
JJA_NDVI	0	0	<b>0.55</b>	0
SON_NDVI	0	0	<b>0.54</b>	0
<b>11. Deciduous Forest and Woodland</b>				
DJF_NDVI	0	0	0	0
MAM_NDVI	0	0	0	0
JJA_NDVI	0	0	<b>0.54</b>	0
SON_NDVI	0	<b>0.46</b>	<b>0.7</b>	0

**Table 2.** The weight fractions of different variables towards explaining the JJA rainfall.

<b>Weight (%)</b>	<b>Parameter</b>
3.98	MAM NDVI
29.17	MAM Soil Moisture
-5.29	JJA Aerosol Optical Depth
0.93	JJA Land Surface Temperature
-2.21	OND Southern Oscillation Index
73.41	JJA Dipole Mode Index